Strong-field quantum control of 2 + 1 photon absorption of atomic sodium

Sangkyung Lee,[1] **Jongseok Lim,**[1] **Chang Yong Park,**[2] **and Jaewook Ahn**[1]

[1] *Department of Physics, KAIST, Daejeon 305-701, Korea*
[2] *Korea Research Institute of Science and Standards, Daejeon 305-340, Korea*

Abstract: We demonstrate ultrafast coherent control of multiphoton absorption in a dynamically shifted energy level structure. In a three-level system that models optical interactions with sodium atoms, we control the quantum interference of sequential 2 + 1 photons and direct three-photon transitions. Dynamic change in energy levels predicts an enormous enhancement of $|7p\rangle$-state excitation in the strong-field regime by a negatively chirped pulse. In addition, the $|4s\rangle$-state excitation is enhanced symmetrically by nonzero linear chirp rates given as a function of laser peak intensity and laser detuning. Experiments performed by ultrafast shaped-pulse excitation of ground-state atomic sodium verifies the various strong-field contributions to $|3s\rangle$-$|7p\rangle$ and $|3s\rangle$-$|4s\rangle$ transitions. The result suggests that for systems of molecular level understanding adiabatic control approach with analytically shaped pulses becomes a more direct control than feedback-loop black-box approaches.

OCIS codes: (190.7110) Ultrafast nonlinear optics; (190.4180) Multiphoton processes; (320.5540) Pulse shaping.

References and links

1. R. S. Judson, H. Rabitz, "Teaching lasers to control molecules," Phys. Rev. Lett. **68**, 1500-1503 (1992).
2. K. Bergmann, H. Theuer, and B. W. Shore, "Coherent population transfer among quantum states of atoms and molecules," Rev. Mod. Phys. **70**, 1003-1025 (1998).
3. M. Shapiro and P. Brumer, *Principles of the quantum control of molecular processes*,(Wiley, New York, 2003).
4. D. J. Tanner and S. A. Rice, "Control of selectivity of chemical reaction via control of wavepacket evolution," J. Chem. Phys. **83**, 5013-5018 (1985).
5. A. M. Weiner, "Femtosecond pulse shaping using spatial light modulators," Rev. Sci. Instrum. **71**, 1929-1960 (2000).
6. D. Goswami, "Optical pulse shaping approaches to coherent control," Phys. Rep. **374**, 385-481 (2003).
7. H. Rabitz, R. de Vivie-Riedle, M. Motzkus, and K. Kompa, "Whither the future of controlling quantum phenomena?" Science **288**, 824-828 (2000).
8. A. Assion, T. Baumert, M. Bergt, T. Brixner, B. Kiefer, V. Seyfried, M. Strehle, and G. Gerber, "Control of chemical reactions by feedback-optimized phase-shaped femtosecond laser pulses," Science **282**, 919 (1998).
9. D. Meshulach and Y. Silberberg, "Coherent quantum control of two-photon transitions by a femtosecond laser pulse," Nature **396**, 239-242 (1998).
10. T. Hournung, R. Meier, D. Zeidler, K.-L. Kompa, D. Proch, and M. Motzkus, "Optimal control of one- and two-photon transitions with shaped femtosecond pulses and feedback," Appl. Phys. B **71**, 277 (2000).
11. Z. Zheng and A. M. Weiner, "Coherent control of second harmonic generation using spectrally phase coded femtosecond waveforms," Chem. Phys. **267**, 161 (2001).
12. D. Meshulach and Y. Silberberg, "Coherent quantum control of multiphoton transitions by shaped ultrashort optical pulse," Phys. Rev. A. **60**, 1287 (1999).
13. Z. Amitay, A. Gandman, L. Chuntonov, and L. Rybak, "Multichannel selective femtosecond coherent control based on symmetry properties," Phys. Rev. Lett. **100**, 193002 (2008).

#139363 - $15.00 USD Received 8 Dec 2010; revised 18 Jan 2011; accepted 18 Jan 2011; published 24 Jan 2011

14. N. Dudovich, B. Dayan, S. M. Gallagher Faeder, and Y. Silberberg, "Transform-limited pulses are not optimal for resonant multiphoton transitions," Phys. Rev. Lett. **86**, 47-50 (2001).
15. N. Dudovich, D. Oron, and Y. Silberberg, "Single-pulse coherently controlled nonlinear Raman spectroscopy and microscopy," Nature **418**, 512 (2002).
16. J. P. Ogilvie, D. Débarre, X. Solinas, J. Martin, E. Beaurepaire and M. Joffre, "Use of coherent control for selective two-photon fluorescence microscopy in live organisms," Opt. Express **14**, 759-766 (2006).
17. T. C. Weinacht, J. Ahn, and P. H. Bucksbaum, "Controlling the shape of a quantum wavefunction," Nature **397**, 233-235 (1999).
18. M. C. Stowe, A. Pe'er, and J. Ye, "Control of four-level quantum coherence via discrete spectral shaping of an optical frequency comb," Phys. Rev. Lett. **100**, 203001 (2008).
19. V. Blanchet, C. Nicole, M.-A. Bouchene, and B. Girard, "Temporal coherent control in two-photon transitions: from optical interferences to quantum interferences," Phys. Rev. Lett. **78**, 2717 (1997).
20. M. A. Bouchene, V. Blanchet, C. Nicole, N. Melikechi, B. Girard, H. Ruppe, S. Rutz, E. Scheriber, L. Wörste, "Temporal coherent control induced by wave packet interferences in one and two photon atomic transitions," Eur. Phys. J. D **2**, 131 (1998).
21. B. Chatel, J. Degert, S. Stock, and B. Girard, "Competition between sequential and direct paths in a two-photon transition," Phys. Rev. A **68**, 041402(R) (2003).
22. S. Lee, J. Lim, and J. Ahn, "Strong-field two-photon absorption in atomic cesium: an analytical control approach," Opt. Express **17**, 7648 (2009).
23. S. Lee, J. Lim, J. Ahn, V. Hakobyan, and S. Guerin, "Strong-field two-photon transition by phase shaping," Phys. Rev. A **82**, 023408 (2010).
24. N. Dudovich, T. Polack, A. Pe'er, and Y. Silberberg, "Simple route to strong-field coherent control," Phys. Rev. Lett. **94**, 083002 (2005).
25. C. Trallero-Herrero, J. L. Cohen, and T. Weinacht, "Strong-field atomic phase matching," Phys. Rev. Lett. **96**, 063603 (2006).
26. H. Suchowski, A. Natan, B. D. Bruner, and Y. Silberberg, "Spatio-temporal coherent control of atomic systems: weak to strong field transition and breaking of symmetry in 2D maps," J. Phys. B:At. Mol. Opt. Phys. **41**, 074008 (2008).
27. E. A. Shapiro, V. Milner, C. Menzel-Jones, M. Shapiro, "Piecewise adiabatic passage with a series of femtosecond pulses," Phys. Rev. Lett. **99**, 033002 (2007).
28. M. Wollenhaupt, A. Präkelt, C. Sarpe-Tudoran, D. Liese, and T. Baumert, "Quantum control by selective population of dressed states using intense chirped femtosecond laser pulses," Appl. Phys. B **82**, 183-188 (2006).
29. S. D. Clow, C. Trallero-Herrero, T. Bergeman, and T. Weinacht, "Strong field multiphoton inversion of a three-level system using shaped ultrafast laser pulses," Phys. Rev. Lett. **100**, 233603 (2008).
30. T. Bayer, M. Wollenhaupt, C. Sarpe-Tudoran, and T. Baumert, "Robust photon locking," Phys. Rev. Lett. **102**, 023004 (2009).
31. P. Meystre and M. SargentIII, *Elements of Quantum Optics, 3rd ed.* (Springer-Verlag, Berlin, 1991).
32. D. A. Steck, *Alkali D Line Data*, http://steck.us/alkalidata/
33. F. Verluise, V. Laude, Z. Cheng, Ch. Spielmann, and P. Tournois, "Amplitude and phase control of ultrashort pulses by use of an acousto-optic programmable dispersive filter: pulse compression and shaping," Opt. Lett. **25**, 575-577 (2000).
34. D. E. Keller, A. E. Kramida, J. R. Fuhr, L. Podobedova, and W. L. WIese, in NIST atomic Spectra database, NIST Standard Reference Database Version 4, http://physics.nist.gov/PhysRefData/ASD/

1. Introduction

In modern laser optics, light is not only a viewing tool, but also a tool for controlling quantum objects and light-induced phenomena [1]. Light with programmed spectral and temporal shapes can be used for quantum-mechanical control of an object by altering the dynamics of the amplitude (probability distribution) and/or the phase (quantum coherence) of the quantum wave function, a method referred to as "quantum control" or "coherent control" [2, 3, 4]. The coherent preparation of light has been considered relatively easy compared with that of matter; therefore, in a light-matter interacting system, the quantum states of the matter are controlled by controlling the coherent nature of the interacting light [5]. Thus, both laser development and light control play important roles in the study of coherent control. Recently, ultrafast lasers, which produce coherent superposition of broadband frequency components in optical regions, have been widely used under various conditions for coherent control experiments. (For a general review, see Ref. [6].) For example, the challenge of optimizing various light-matter interactions

#139363 - $15.00 USD Received 8 Dec 2010; revised 18 Jan 2011; accepted 18 Jan 2011; published 24 Jan 2011

has been addressed with designed laser pulses by either solving the Schrödinger equation or by feedback adaptation [2, 7]. Feedback adaptive coherent control, or closed-loop control, was first demonstrated with photo-dissociation by Gerber and coworkers [8]. Also, in the same year, Meschulach and Silberberg optimized two-photon absorption by designing ultrafast, short optical control pulses [9]. Both of these methods for ultrafast coherent control have been applied to the optimization of nonlinear processes (e.g., second-harmonic generation, third-harmonic generation [10, 11], and multiphoton absorption [12, 13, 14]), nonlinear Raman spectroscopy (CARS) [15], *in-vivo* fluorescence microscopy [16], and coherent manipulation of Rydberg atoms [17] and cole atoms [18].

In particular, ultrafast coherent control in multiphoton absorption has been studied widely in the weak-field regime because the Hamiltonian for the given light-matter interaction is relatively simple to solve analytically. As the energy-level structure of the matter remains unchanged in the weak-field interaction regime, analytic forms are obtained from perturbation theory. For example, multiphoton processes with pulses of π phase step, sinusoidal phase [13, 14, 18], and linear chirping [19, 20, 21] have been considered. However, further enhancement of the optical processes requires a study in the strong-field interaction regime [22, 23], in which strong-field effects, such as the dynamic Stark shift and power broadening, must be considered. It is now well known that the control schemes devised in the weak-field regime are not always directly applicable to strong-field coherent control, although there are exceptions. For example, power broadening can be compensated in part by the solution of the weak-field regime [24]. Recently, there have been many studies on strong-field coherent control. For the optimization of strong-field two-photon absorption, Weinacht and coworkers proposed strong-field atomic phase matching [25], and the Silberberg group phenomenologically studied strong-field two-photon absorption using spectro-temporal two-dimensional maps [26]. There was an attempt to maximize two-photon absorption using the piecewise linear chirped pulse [27]. For selection of the desired state among accessible states, the selective population of dressed states was demonstrated based on adiabatic passages and photon locking [28]. In terms of selective excitation in alkali atoms, the population inversion in the sodium three-level system has been demonstrated using the GA algorithm [29], and the selective population transfer of dressed states using the AC stark shifts has been studied in atomic potassium [30].

In this paper, we report an experimental study of ultrafast coherent control of multiphoton absorption in a dynamically shifted energy-level structure. In a three-level system modeled for ultrafast optical interactions with ground-state sodium atoms, we controlled the quantum interference of sequential 2 + 1 photons and direct three-photon transitions. The dynamic structural change of sodium energy levels predicts an enormous enhancement of $|7p\rangle$-state excitation by a negatively chirped pulse in the strong-field regime. In addition, the $|4s\rangle$-state excitation is enhanced symmetrically by nonzero linear chirp rates given as a function of laser peak intensity and laser detuning. We first obtained analytical formulas for the strong-field contributions to $|3s\rangle$-$|7p\rangle$ and $|3s\rangle$-$|4s\rangle$ transitions and then verified them by experiments performed with programmed laser pulses.

2. Theoretical considerations

We consider a three-state model system to describe the ultrafast optical interaction of ground-state atomic sodium. The first two energy states are two-photon states coupled with each other, and the third is a one-photon state that is resonant with the second state. The effective Hamiltonian in the resonant approximation can be written in terms of the three states $\{|g\rangle, |e\rangle, |f\rangle\}$

#139363 - $15.00 USD Received 8 Dec 2010; revised 18 Jan 2011; accepted 18 Jan 2011; published 24 Jan 2011

as [31]

$$\hat{H}(t) = \begin{pmatrix} S_g(t) & \frac{1}{2}\Omega(t)e^{i[\Delta_1 t+2\phi(t)]} & 0 \\ \frac{1}{2}\Omega(t)e^{-i[\Delta_1 t+2\phi(t)]} & S_e(t) & \frac{1}{2}\Omega_{ef}(t)e^{i[\Delta_2 t+\phi(t)]} \\ 0 & \frac{1}{2}\Omega_{ef}(t)e^{-i[\Delta_2 t+\phi(t)]} & S_f(t) \end{pmatrix}, \quad (1)$$

where $S_g(t)$, $S_e(t)$, and $S_f(t)$ represent the dynamic Stark shifts, $\Omega(t)$ and $\Omega_{ef}(t)$ are the two-photon and one-photon Rabi frequencies, respectively, Δ_1 is the two-photon detuning defined by $\Delta_1 = 2\nu - \omega_e + \omega_g$, and Δ_2 is the one-photon detuning, $\Delta_2 = \nu - \omega_f + \omega_e$, where ω_g, ω_e, and ω_f are the respective energies of the $|g\rangle$, $|e\rangle$, and $|f\rangle$ states. $\phi(t)$ is the phase of the laser field relative to its central frequency, ν. The Hamiltonian can be alternatively expressed as

$$\hat{H}^{(T)}(t) = \begin{pmatrix} S_g(t)+\Delta_1+2\dot{\phi}(t) & \frac{1}{2}\Omega(t) & 0 \\ \frac{1}{2}\Omega(t) & S_e(t) & \frac{1}{2}\Omega_{ef}(t) \\ 0 & \frac{1}{2}\Omega_{ef}(t) & S_r(t)-\Delta_2-\dot{\phi}(t) \end{pmatrix}, \quad (2)$$

using the transformation $\hat{H}^{(T)} = \hat{T}^{\dagger}\hat{H}\hat{T} - i\hbar\hat{T}^{\dagger}d\hat{T}/dt$, where $\hat{T} = e^{i[\Delta_1 t+2\phi(t)]}|g\rangle\langle g| + |e\rangle\langle e| + e^{-i[\Delta_2 t+\phi(t)]}|f\rangle\langle f|$. Furthermore, the transformation matrix $\hat{T}' = e^{-i\left[\int^t S_g(u)du+\Delta_1 t+2\phi(t)\right]}|g\rangle\langle g| + e^{-i\int^t S_e(u)du}|e\rangle\langle e| + e^{-i\left[\int^t S_f(u)du-\Delta_2 t-\phi(t)\right]}|f\rangle\langle f|$ transforms the diagonal terms in Eq. (2) into the off-diagonal phase terms, making the Hamiltonian

$$\hat{H}^{(T')}(t) = \begin{pmatrix} 0 & \frac{1}{2}\Omega(t)e^{iQ_1(t)} & 0 \\ \frac{1}{2}\Omega(t)e^{-iQ_1(t)} & 0 & \frac{1}{2}\Omega_{ef}(t)e^{iQ_2(t))} \\ 0 & \frac{1}{2}\Omega_{ef}(t)e^{-iQ_2(t)} & 0 \end{pmatrix}, \quad (3)$$

where $Q_1(t) = -\int^t S_{eg}(u)du + \Delta_1 t + 2\phi(t)$ and $Q_2(t) = -\int^t S_{fe}(u)du + \Delta_2 t + \phi(t)$. $S_{eg}(t)$ and $S_{fe}(t)$ are the level-shift parameters given as $S_{eg}(t) = S_e(t) - S_g(t)$ and $S_{fe}(t) = S_f(t) - S_e(t)$.

Neither transformation chang the state populations, and the probability amplitudes, aside from the global phase factors, can be calculated in the perturbative regime that satisfies $\Omega(t)\tau \ll 1$ and $\Omega_{ef}(t)\tau \ll 1$. For the $|f\rangle$ state, the probability amplitude is given as the second-order Dyson series:

$$a_f = \int_{-\infty}^{\infty} dt \frac{\Omega_{ef}(t)}{2} e^{-iQ_2(t)} \int_{-\infty}^{t} dt' \frac{\Omega(t')}{2} e^{-iQ_1(t')}, \quad (4)$$

where $Q_1(t)$ and $Q_2(t)$ are the atomic phases induced from laser detuning, level shift, and the temporal phase of laser pulses. The probability amplitude of the $|e\rangle$ state is given by

$$\begin{aligned} a_e &= -i\int_{-\infty}^{\infty} dt \frac{\Omega(t)}{2} e^{-iQ_1(t)} \\ &+ i\int_{-\infty}^{\infty} dt \frac{\Omega_{ef}(t)}{2} e^{-iQ_2(t)} \int_{-\infty}^{t} dt' \frac{\Omega_{ef}(t')}{2} e^{iQ_2(t')} \int_{-\infty}^{t'} dt'' \frac{\Omega(t'')}{2} e^{-iQ_1(t'')}, \end{aligned} \quad (5)$$

where the dominant contribution is from the two-photon excitation in a decomposed two-level system in $|g\rangle$, $|e\rangle$ bases.

The optimal excitation of each $|e\rangle$ and $|f\rangle$ state is determined by the engineered quantum interference of the transition probabilities. In the following section, we discuss the derivation and testing of approximate behaviors of the excited energy levels of atomic sodium induced by shaped pulses, especially in the strong-field interaction regime where the structure of the energy levels is strongly altered during the pulse interaction.

#139363 - $15.00 USD Received 8 Dec 2010; revised 18 Jan 2011; accepted 18 Jan 2011; published 24 Jan 2011

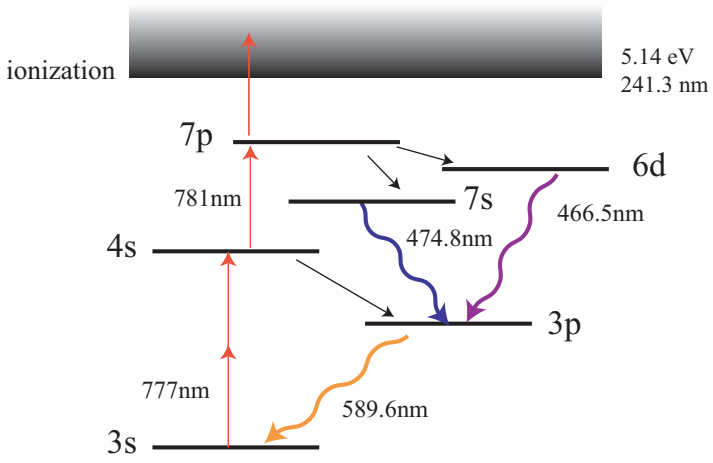

Fig. 1. Energy levels and transitions of atomic sodium

3. Experimental

The energy-level structure of atomic sodium is shown in Fig. 1, where the ground-state atoms are excited to the $|4s\rangle$ energy-state by non-resonant two-photon absorption of 777-nm light. The energy difference between the $|4s\rangle$ and $|7p\rangle$ states is 781 nm, and the transition between these states is single-photon resonant with the laser light. Because the atoms interacted with a sub-picosecond optical pulse of broad wavelengths, including both resonant wavelengths, 777 and 781 nm, the $|4s\rangle$ and $|7p\rangle$ states were simultaneously excited. The resulting wave function is a coherent superposition state of $|3s\rangle$, $|4s\rangle$, and $|7p\rangle$. Sodium atoms were prepared in a heated optical cell. The vapor pressure of sodium in the solid phase is given by [32] $\log_{10} P_v = 2.881 + 5.298 - 5603/T$, where the temperature, T, is in Kelvin, and the vapor pressure, P_v, is in Torr; thus, the density of sodium atoms was $2.0 \times 10^{17}/m^3$ in the heated cell at 423 K. The lifetimes of the excited sodium atoms are on the order of a few tens of nanoseconds. The ionization probability at the explored laser intensity of 10^{13} W/cm^2 was 1000 times smaller than the $|4s\rangle - |7p\rangle$ transition. For the interaction of sodium atoms with short optical pulses of a few picoseconds, the decay processes and ionization processes could be ignored during the excitation; therefore, the $|3s\rangle$, $|4s\rangle$, and $|7p\rangle$ energy states formed the three-state model system under consideration.

For the generation and pulse shaping of sub-picosecond optical pulses, we used a Ti:sapphire laser amplifier system that produced 50-fs short optical pulses. The laser was operated at a 1-kHz repetition rate, and the central wavelength was tuned between 779 and 800 nm. The optical pulses of 100-μJ of energy were shaped by an actively controlled acousto-optic programmable dispersive filter [33] inserted into the laser system between the amplifier gain medium and the pulse compressor. The shaped pulses were spatially filtered and then focused in a vapor cell of sodium atoms. The beam radius at the focus was 32.8 μm, and the Rayleigh range was 4.0 mm. The focused spot in the vapor cell was imaged by a telescope, and the fluorescence was collected by a photomultiplier (PMT, Hamamatsu R1527P). The two-photon Rabi coupling was $\Omega(0)$=-10.25 Trad/s at the laser peak, and the Rabi coupling between the $|4s\rangle$ and $|7p\rangle$ states was $\Omega_{er}(0) = 5.45$ Trad/s. For the two-photon rotating wave approximation, we verified that $|\Delta| \ll \omega_{jg} - \nu \simeq \omega_{je} + \nu$. At a 777-nm center wavelength, the two-photon detuning was nearly zero, and the given condition was satisfied. At 800 nm, $|\Delta| \approx 140\times$ Trad/s and $\omega_{jg} - \nu \gg$

#139363 - $15.00 USD Received 8 Dec 2010; revised 18 Jan 2011; accepted 18 Jan 2011; published 24 Jan 2011

700× Trad/s, so the approximation condition was satisfied.

To record the $|7p\rangle$ excited population, we used the $|7s\rangle$-$|3p\rangle$ transition. (Fig. 1) The 475-nm fluorescence signal was measured as a function of the control parameters of the shape programming. In addition, the $3p\rangle - |3s\rangle$ transition signal was used for the combined sum of $|7p\rangle$ and $|4s\rangle$ populations, both of which were excited by shaped laser pulses. We note that the Einstein coefficients were $A_{7p-3s} = 7.96 \times 10^4/s$ and $A_{7p-7s} = 1.70 \times 10^5/s$, and 57% of the $|7p\rangle$ population reached the $|3p\rangle$ state [34]. The fluorescence signals were centered at 590 nm and 475 nm for the $|7s\rangle$-$|3p\rangle$ and $|3p\rangle$-$|3s\rangle$ transitions, respectively, and were individually collected via spectral bandpass filters placed in front of the PMT. The signal intensity of the PMT was kept in the well-calibrated linear detection range, and the $|7p\rangle$ excited state, maintained below the saturation limit, was linearly mapped with the fluorescence signal.

4. Results and discussion

The Gaussian pulse width T_0 of a transform-limited pulse is about 37 fs. For a linearly chirped pulse which interacts with Sodium atoms, actual Gaussian pulse width is given by $\tau = T_0\sqrt{1+(2a_2/T_0^2)^2}$, where a_2 is chirp rate in frequency-domain. In time-domain, the frequency sweeping of a linearly chirped pulse is given as a function of time by $\dot{\phi}(t) = 2\beta t$, where $\beta = 2a_2/\left(\tau^2 T_0^2\right)$. In our experiments, the shaped chirped pulses have the same spectrum and also the same fixed energy. Because of the fixed pulse energy in our experiments, the peak intensity of the linearly chirped pulse is reduced by $\tau(a_2)/T_0$ times relative to that of a transform-limited pulse. Thus, the dynamic Stark shifts induced by linearly chirped pulses become smaller than those by a transform limited pulse.

4.1. Control of sodium $|7p\rangle$-state excitation

Figure 2 shows a dressed-state picture of the given 2 + 1 photon absorption processes in the sodium three-state model system. First, we considered the transition paths from the $|3s\rangle$ to $|f\rangle = |7p\rangle$ states. Three possible paths are indicated in Fig. 2(a). For a positively chirped pulse, the photon frequency increased as a function of time; therefore, the $|3s\rangle - |7p\rangle$ transition was possible along path (III), which is a direct transition path from $|3s\rangle$ to $|7p\rangle$ that does not pass by the $|4s\rangle$ state. On the other hand, for a negatively chirped pulse, the photon frequency decreased, and two paths are possible: a sequential path (I) and a direct path (II). Considering the fact that path (III) is an inefficient excitation, it is thought that the $|7p\rangle$ atoms were generated more effectively by a negatively chirped pulse than by a positively chirped pulse.

This asymmetric excitation to the $|7p\rangle$ state, obtained as a function of the chirp parameter, can be understood in a time-frequency schematic. Figures 2(b) and (c) show one-photon (red) and two-photon (blue) spectrograms of chirped laser pulses that are plotted in two-dimensional time space and frequency. They are overlaid with the resonant frequency shifts of $|4s\rangle$-$|7p\rangle$ and $|3s\rangle$-$|4s\rangle$ transitions (dashed lines). Figure 2(b) shows that the $|3s\rangle$-$|4s\rangle$ transition occurred first and the $|4s\rangle$-$|7p\rangle$ occurred later; thus, a sequential excitation along the $|3s\rangle \rightarrow |4s\rangle \rightarrow |7p\rangle$ path was satisfied. On the other hand, for a positively chirped pulse shown in Fig. 2(c), because the $|3s\rangle$-$|4s\rangle$ resonance frequency was up-shifted during the optical interaction, the two-photon spectrum overlaps with the resonance line after the temporal center of the pulse. As a result, the $|3s\rangle$-$|4s\rangle$ and $|4s\rangle$-$|7p\rangle$ transitions occurred in a time-reversal sequence, indicating that the sequential excitation was not possible. Thus, sequential excitation is not possible for a positively chirped pulse, and only non-sequential excitations, e.g., along path (III) in Fig. 2(a), are possible.

In the following sub-section, we use the theoretical model described in Sec. II to calculate the sequential and non-sequential excitations to the $|7p\rangle$ state and verify the results with corre-

#139363 - $15.00 USD Received 8 Dec 2010; revised 18 Jan 2011; accepted 18 Jan 2011; published 24 Jan 2011

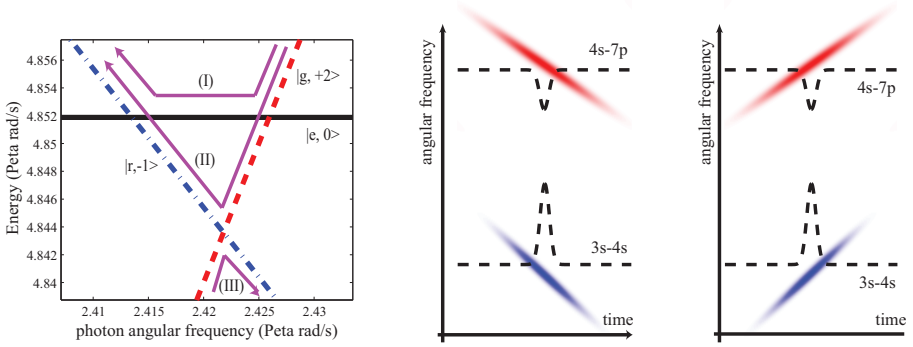

(a) Dressed States of Atomic Sodium (b) Negative Chirp (c) Positive Chirp

Fig. 2. (a) Dressed-state picture for a 2 + 1 photon absorption process in a sodium three-state model system. Three arrows indicate possible transition paths from $|g\rangle$ to $|r\rangle$ for a negatively chirped pulse interaction. (b) Schematic illustrations of dynamically Stark-shifted resonant frequencies of $|3s\rangle - |4s\rangle$ and $|4s\rangle - |7p\rangle$ transitions (dashed lines) of sodium atoms, overlaid with two-photon (blue) and one-photon (red) time-frequency spectrograms for the negatively chirp pulse of $a_2 = -5000$ fs^2. (c) Similar illustration for a positively chirped pulse with $a_2 = 5000$ fs^2. The spectrograms were vertically shifted to match the corresponding transitions.

sponding experiments.

4.2. *Calculation of the sequential and direct $|7p\rangle$ excitations*

The probability amplitude of the $|7p\rangle$ state is obtained from Eq. (4). To calculate the transition probability amplitudes for the sequential and direct excitation paths, we separated Eq. (4) into two parts: resonant and non-resonant. In the perturbative interaction regime, the probability amplitudes corresponding to these two parts can be written, respectively, as [25]:

$$a_{\mathrm{f,res}} = i\pi E(\omega_{re}+\delta_{fe})\int_{-\infty}^{\infty} d\omega E(\omega)E(\omega_{eg}+\delta_{eg}-\omega), \tag{6}$$

$$a_{\mathrm{f,nonres}} = \wp\int_{-\infty}^{\infty} d\omega \frac{E(\omega)}{\omega-\omega_{fe}-\delta_{fe}}\int_{-\infty}^{\infty} d\omega' E(\omega')E(\omega_{fg}+\delta_{fg}-\omega-\omega'), \tag{7}$$

where $\wp$ is the Cauchy principal value. The subscripts "res" and "nonres" denote the resonant and non-resonant excitations, and δ_{eg} and (δ_{fe} are the maximum amplitudes of the total level shifts of the $|3s\rangle - |4s\rangle$ and $|7p\rangle - |4s\rangle$ transitions, respectively, which are calculated at the temporal peak of a transform-limited pulse. $E(\omega)$ is the Fourier transform of the electric field profile, a spectrally chirped Gaussian pulse, given by

$$E(\omega) = \sqrt{\pi}E_o T_o \exp\left(-\frac{1}{4}(\omega-\nu)^2 T_o^2 + ia_2(\omega-\nu)^2\right), \tag{8}$$

where T_o is the Gaussian width of a transform-limited pulse, and a_2 is the linear chirp parameter in the spectral domain.

The resonant $|3s\rangle \rightarrow |7p\rangle$ excitation was obtained by substituting Eq. (8) into Eq. (6) as

$$a_{\mathrm{f,res}} = \sqrt{\frac{2\pi^3}{T_o T_p}}E^2(\nu)\exp\left[-\left(\frac{\delta_{1\mathrm{ph}}^2(\nu)}{4}+\frac{\delta_{2\mathrm{ph}}^2(\nu)}{8}\right)(T_o^2+2ia_2)\right]e^{i(\theta+\pi)/2}, \tag{9}$$

#139363 - $15.00 USD Received 8 Dec 2010; revised 18 Jan 2011; accepted 18 Jan 2011; published 24 Jan 2011

where $\tan\theta = -2a_2/T_o^2$, the two-photon detuning, is defined as $\delta_{2\mathrm{ph}}(\nu) = \omega_{eg} + \delta_{eg} - 2\nu$, and the one-photon detuning is defined as $\delta_{1\mathrm{ph}}(\nu) = \omega_{fe} + \delta_{fe} - \nu$. Alternatively, Eq. (9) can be written as

$$a_{\mathrm{f,res}} = \sqrt{\frac{2\pi^3}{T_o T_p}} E^2(\nu) \exp\left[-\left(\frac{\delta_{3\mathrm{ph}}^2(\nu)}{12} + \frac{3\delta_s^2}{8} \right) (T_o^2 + 2ia_2) \right] e^{i(\theta+\pi)/2}, \tag{10}$$

where three-photon detuning is defined as $\delta_{3\mathrm{ph}}(\nu) = \omega_{fg} + \delta_{fg} - 3\nu$, and δ_{s} is the structure factor, $\delta_{\mathrm{s}} = \omega_{fe} + \delta_{fe} - (\omega_{fg} + \delta_{fg})/3$ that is independent of ν.

The transition probability for the resonant excitation to $|7p\rangle$ is the absolute square of Eq. (10). The result is a symmetric function of chirp a_2, which contradicts the prediction in Sec. 4.1 that the sequential excitation should be an asymmetric function of the chirp. However, there is indeed another sequential path in the non-resonant excitation path in Eq. (7). Although the resonant excitation ($a_{\mathrm{f,res}}$) contributed only to the sequential transition path ($|3s\rangle \rightarrow |4s\rangle \rightarrow |7p\rangle$), the non-resonant part ($a_{\mathrm{f,nonres}}$) contributed to both the sequential and direct paths, i. e.,

$$a_{\mathrm{f}} = a_{\mathrm{f,res}}^{\mathrm{seq}} + a_{\mathrm{f,nonres}}^{\mathrm{seq}} + a_{\mathrm{f,nonres}}^{\mathrm{direct}}, \tag{11}$$

where $a_{\mathrm{f,res}}^{\mathrm{seq}} = a_{\mathrm{f,res}}$ because there were no resonant non-sequential transitions.

For the calculation of the non-resonant direct excitation $a_{\mathrm{r,nonres}}^{direct}$, we considered Eq. (7) near the three-photon resonant condition, i.e., $\omega \approx (\omega_{fg} + \delta_{fg})/3$. Then, the denominator of the integrand in Eq. (7) can be treated as a constant, and it is simple to show that

$$a_{\mathrm{f,nonres}}^{\mathrm{direct}} = -\frac{4\pi}{\sqrt{3}\delta_s T_o T_p} E^3(\nu) \exp\left[-\frac{\delta_{3\mathrm{ph}}^2}{12} (T_o^2 + 2ia_2) \right] e^{i\theta}. \tag{12}$$

Finally, for the calculation of $a_{\mathrm{r,nonres}}^{\mathrm{seq}}$, we considered the small frequency range around the pole, i.e., $\omega \approx \omega_{fe} + \delta_{fe}$, in Eq. (7). Equation (7) is written as

$$\begin{aligned} a_{\mathrm{f,nonres}}^{\mathrm{seq}} &= \sqrt{\frac{2\pi}{T_o T_p}} E^3(\nu) \exp\left[-\frac{\delta_{3ph}^2}{12} (T_o^2 + 2ia_2) \right] e^{i\theta/2} \\ &\times \wp \int_{-\infty}^{\infty} \frac{d\omega}{\omega - \omega_{fe} - \delta_{fe}} \exp\left[-\frac{3}{8} \left(\omega - \frac{\omega_{fg} + \delta_{rg}}{3} \right)^2 (T_o^2 + 2ia_2) \right]. \end{aligned} \tag{13}$$

By neglecting the term of the order of $O(\omega - \omega_{fe} + \delta_{fe})^2$, the non-resonant sequential excitation is given by

$$\begin{aligned} a_{\mathrm{f,nonres}}^{\mathrm{seq}} &= \sqrt{\frac{2\pi^3}{T_o T_p}} E^2(\nu) \exp\left[-\left(\frac{\delta_{3\mathrm{ph}}^2(\nu)}{12} + \frac{3\delta_s^2}{8} \right) (T_o^2 + 2ia_2) \right] e^{i(\theta+\pi)/2} \mathrm{sgn}(a_2\delta_s) \\ &= a_{\mathrm{f,res}}^{\mathrm{seq}} \mathrm{sgn}(a_2\delta_s), \end{aligned} \tag{14}$$

where the sign function, defined by sgn(x)=+1 (-1) for $x > 0$ ($x < 0$), is due to the contour integral given as a function of the sign of $\delta_s a_2$. The result is valid in the chirp range of $|a_2|/T_o^2 \gg 1$. In the experiment, T_o is 37 fs, and the approximation $|a_2|/T_o^2 \gg 1$ was valid for $|a_2| >$ 1369 fs^2. In sodium, δ_s= -8.3 Trad/s, and as a result, $a_{\mathrm{f,nonres}}^{\mathrm{seq}} + a_{\mathrm{f,res}}^{\mathrm{seq}} = 0$ for $a_2 > 0$. Therefore, the net sequential excitation path to $|7p\rangle$ in Eq. (11) vanishes for a positively chirped pulse because the resonant and non-resonant contributions cancel each other.

#139363 - $15.00 USD Received 8 Dec 2010; revised 18 Jan 2011; accepted 18 Jan 2011; published 24 Jan 2011

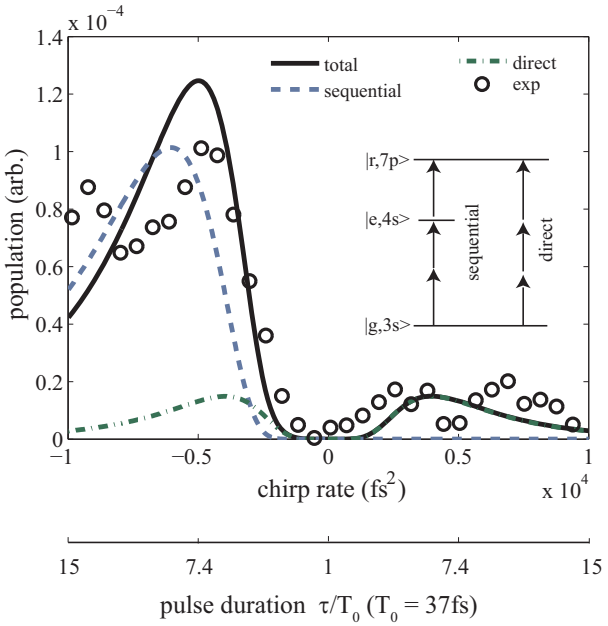

Fig. 3. Three-photon sodium excitation to the $|7p\rangle$ state with a chirped optical pulse. The curves show the calculation of total (solid line), sequential (blue dashed line), and direct (green dot-dash line) transitions. The experimental measurements are shown as circles. The inset shows the sequential and direct transition paths from $|3s\rangle$ to $|7p\rangle$.

4.3. Verification of shaped-pulse $|7p\rangle$-state excitation

The sodium $|7p\rangle$ excitation was experimentally tested as a function of the chirp rate a_2. Figure 3 shows the calculation of the net transition probability (solid line) of $|3s\rangle - |7p\rangle$ given in Eq. (11), the components of which were obtained from Eq. (10), Eq. (12), and Eq. (14) as a function of the linear chirp rate. The laser (transform-limit) peak intensity was kept at $I = 3.0 \times 10^11$ W/cm^2, and the chirp rate a_2 was varied in the range [-1.0, 1.0]$\times 10^4$ fs^2. As predicted in the schematic picture in Sec. 4.1, the excitation was significantly enhanced by negatively chirped pulses because the sequential excitation path along $|3s\rangle - |4s\rangle - |7p\rangle$ was zero for positively chirped pulses. The direct transition from $|3s\rangle - |7p\rangle$, which is a symmetric function in Eq. (12), was 10 times smaller than the sequential transition for the tested laser peak intensity. For comparison, the sequential and direct excitation probabilities are plotted using dashed and dot-dash lines, respectively. For the numerical calculation, the dynamic Stark shift of the $|3s\rangle$ state was $S_g = -32.8(I/I_o)$ Trad/s, determined by couplings with $|p\rangle$ states, where I_o is the reference laser intensity, $I_o = 1.0 \times 10^{11}$ W/cm^2. The shift of the $|4s\rangle$ state was $S_e = 28.9(I/I_o)$ Trad/s at the same intensity. Thus, the net frequency shift of the two-photon transition was positive. The $|7p\rangle$ state was shifted by couplings with the $|s\rangle$ and $|d\rangle$ states as well as with continuum states. It is known that the presence of a continuum increases the energy of the excited state by the ponderomotive energy given by $S_r(t) = e^2E^2(t)/4mv^2$, where v is the laser frequency, and m is the mass of an electron. As a result, the $|7p\rangle$ state was up-shifted $S_r = 8.7(I/I_o)$ Trad/s, and the net frequency shift of the $|4s\rangle$-$|7p\rangle$ transition was negative $S_{re} = -20.2(I/I_o)$ Trad/s. Also, because the laser beam had a Gaussian spatial intensity distribution, the total excitation probability was calculated as the sum of local excitations, i.e., $P_{\text{total}} = \int_0^\infty P(I(r))d^3r$.

#139363 - $15.00 USD Received 8 Dec 2010; revised 18 Jan 2011; accepted 18 Jan 2011; published 24 Jan 2011

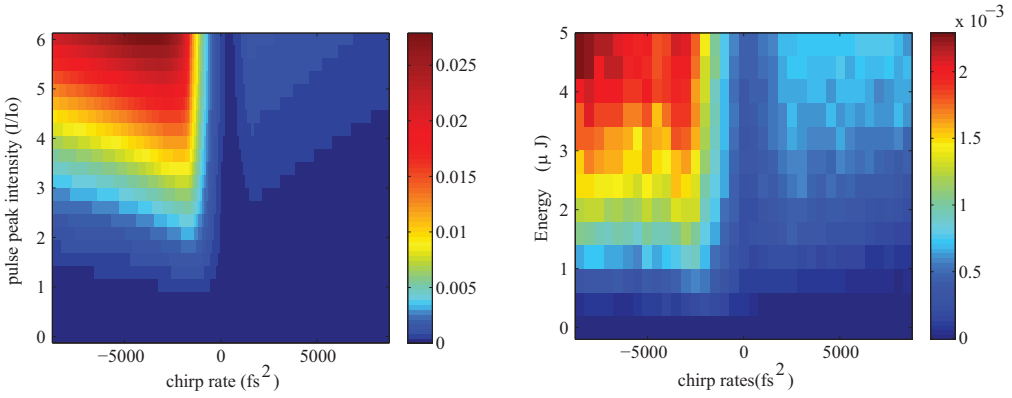

Fig. 4. (a) Theoretical and (b) experimental results of chirped-pulse three-photon excitation probability of sodium atoms as a function of the linear chirp rate and laser peak intensity. For the relative measurement of $|7p\rangle$ sodium atoms, the $|7s\rangle - |3p\rangle$ fluorescence signal was recorded.

The excitation probability calculated as a function of a_2 and laser peak intensity I is compared with the experimentally tested results in Fig. 4. The $|7p\rangle$ excited atoms were measured by monitoring the $|7s\rangle - |3p\rangle$ fluorescence as a function of laser (transform-limited) peak intensity and the chirp parameter (a_2). The laser peak intensity, I, was varied from zero to $I = 6.0 \times 10^{11}$ W/cm^2, and a_2 was varied in the range of [-1.0, 1.0]$\times 10^4$ fs^2. The net transition probability, which is the sum of the calculated sequential and direct transitions shown in Fig. 4(a), showed excellent agreement with the experimental results in Fig. 4(b).

4.4. *Chirped-pulse excitation of* $|4s\rangle$*-state atoms*

Finally, we considered the excitation of $|4s\rangle$ atoms. Figure 5 shows the calculation and experimental results of the excitation probability of $|4s\rangle$-state atoms. It is evident from Eq. (5) that the dominant excitation to the $|4s\rangle$ state was the direct two-photon absorption from the $|3s\rangle$ state. The presence of the $|7p\rangle$ state affected this excitation in terms of the third-order Dyson series, and the new excitation path was a four-photon sequential excitation along $|3s\rangle \rightarrow |4s\rangle \rightarrow |7p\rangle \rightarrow |4s\rangle$. Therefore, the excitation probability amplitude of $|4s\rangle$ atoms is given by

$$a_e = a_e^{\text{direct}} + a_e^{\text{seq}}, \tag{15}$$

where the direct two-photon transition a_e^{direct} is

$$a_e^{\text{direct}} = -i \int_{-\infty}^{\infty} dt \frac{\Omega(t)}{2} e^{-iQ_1(t)}, \tag{16}$$

, and the sequential two-photon transition a_e^{seq} is

$$a_e^{\text{seq}} = i \int_{-\infty}^{\infty} dt \frac{\Omega_{er}(t)}{2} e^{-iQ_2(t)} \int_{-\infty}^{t} dt' \frac{\Omega_{er}(t')}{2} e^{iQ_2(t')} \int_{-\infty}^{t'} dt'' \frac{\Omega(t'')}{2} e^{-iQ_1(t'')}. \tag{17}$$

The probability amplitude of the excitation along the direct transition path is

$$a_e^{direct} = \sqrt{\frac{2\pi}{T_o T_p}} \exp\left[-\frac{\delta_{2ph}^2(\nu)}{8} (T_o^2 + 2ia_2) \right] e^{i(\theta+\pi)/2}, \tag{18}$$

#139363 - $15.00 USD Received 8 Dec 2010; revised 18 Jan 2011; accepted 18 Jan 2011; published 24 Jan 2011

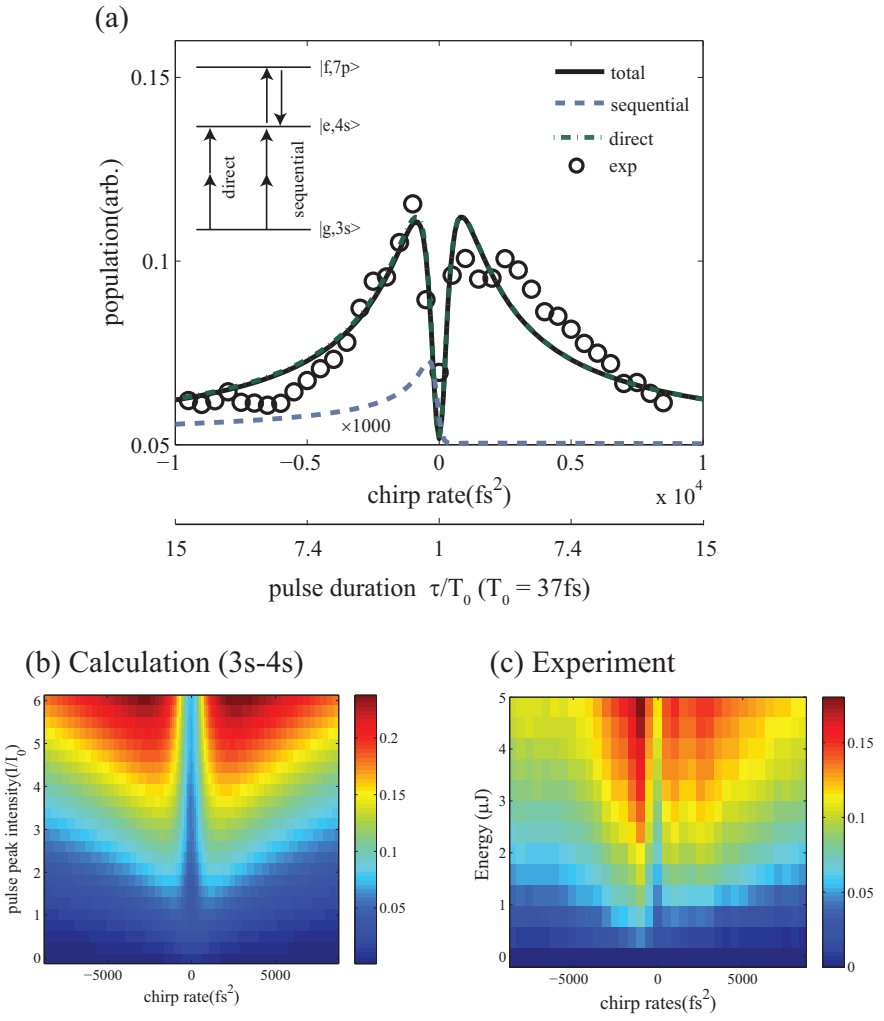

Fig. 5. Chirped-pulse excitation of $|4\rangle$-state sodium atoms. (a) The excitation transition probability shown as a function of chirp rate at a laser transform-limited peak intensity of $I = 3.0 \times 10^{11}$ W/cm^2. The curves show the calculation of total (solid line), sequential (dashed line), and direct (dot-dash line) transitions. The sequential transition was multiplied by 1000. The experimental results are plotted as circles. The inset shows the sequential and direct transition paths from $|3s\rangle$ to $|7p\rangle$. (b) Theoretical and (c) experimental results of the chirped-pulse excitation probability of sodium $|4s\rangle$ atoms plotted as a function of the linear chirp rate and laser peak intensity.

#139363 - $15.00 USD Received 8 Dec 2010; revised 18 Jan 2011; accepted 18 Jan 2011; published 24 Jan 2011

which was the dominant contribution to the net excitation, and the sequential transition via the $|7p\rangle$ state is negligible. Therefore, the excitation probability is given by

$$P_e \simeq |a_e^{direct}|^2 \propto \frac{1}{\sqrt{1+B^2}} \exp\left[-\frac{A^2}{2(1+B^2)}\right], \tag{19}$$

where $A = \delta_{2ph}(\nu)\tau$, and $B = 2a_2/\tau_0^2$. The net excitation probability was a symmetric function of the linear chirp rate and nearly vanished at zero chirp. The dynamic Stark shift of the $|3s\rangle$-$|4s\rangle$ transition caused off-resonance to the two-photon excitation. As the dynamic Stark shift, which is stored in the parameter A, increased, the term $\exp\left(-A^2/(2(1+B^2))\right)$ became important, and the net probability had a local minimum at a chirp rate of zero.

For experiments, the direct two-photon transition a_e^{direct} was the dominant contribution. The direct transition, plotted as a solid line in Fig. 5(a), was symmetric around the zero chirp rate because the direct transition path was available for both negatively and positively chirped pulses. The probability of the $|4s\rangle$ state was determined by the sum of the contributions of the sequential and direct paths, but the sequential transition, dotted lines in Fig. 5(a), only contributed at negative chirp rates and was 1000 times smaller than the direct transition. The calculated excitation probability, given as a function of the linear chirp rate of the shaped pulses at various peak intensities in Fig. 5(b), showed good agreement with the experimental data in Fig. 5(c). A dip was observed at the zero chirp rate. In the experiment, because the pulse energy was fixed, the pulse duration (pulse peak intensity) was shortest (maximum) at the zero chirp rate. The strong peak intensity at the zero chirp rate induced strong off-resonance, reducing the absorption, as expected from Eq. (19). The net excitation probability showed a nearly symmetric function of chirp rate and nearly vanished at zero chirp.

5. conclusion

In conclusion, we theoretically analyzed and experimentally demonstrated 2 + 1 multiphoton absorption in a three-level system in the strong-field regime. In experiments with atomic sodium, we engineered quantum interference between sequential and non-sequential excitation paths from the ground $|3s\rangle$ state to the $|7p\rangle$ state. The dressed-state picture for the three-photon interaction with the three-level model system predicted that the resonant and non-resonant contributions in the sequential excitation interfered destructively and canceled each other for positively chirped pulses. Both analytic formulas and experimental results showed that a negatively chirped pulse enhanced the $|7p\rangle$ population because the sequential path was opened by a negatively chirped pulse. In addition, the $|4s\rangle$-state excitation was enhanced symmetrically by nonzero linear chirp rates given as a function of laser peak intensity and laser detuning. Experiments verified the various strong-field contributions to $|3s\rangle$-$|7p\rangle$ and $|3s\rangle$-$|4s\rangle$ transitions. The transition amplitude formulas analytically obtained by considering the atomic Hamiltonian showed good agreement with the experiment. The result suggests that adiabatic control approach with analytically shaped pulses provides a more direct control of systems of molecular level understandings than feedback-loop black-box approaches do.

Acknowledgments

This research was supported in part by Basic Science Research Program (No. 2009-0090843), and in part by Mid-career Researcher Program (No. 2010-0013899) both through the National Research Foundation of Korea (NRF) funded by the Ministry of Education, Science and Technology . The authors kindly acknowledge Stéphane Guérin for for the comments on the manuscript.

#139363 - $15.00 USD Received 8 Dec 2010; revised 18 Jan 2011; accepted 18 Jan 2011; published 24 Jan 2011